EARTH SURFACE PROCESSES AND LANDFORMS
Earth Surf. Process. Landforms **42**, 1155–1170 (2017)

Published online 4 December 2016 in Wiley Online Library
(wileyonlinelibrary.com) DOI: 10.1002/esp.4079

Plateau reduction by drainage divide migration in the Eastern Cordillera of Colombia defined by morphometry and ^{10}Be terrestrial cosmogenic nuclides

Lucía Struth,[1]* Antonio Teixell,[1] Lewis A. Owen[2] and Julien Babault[1]
[1] Departament de Geologia, Universitat Autònoma de Barcelona, 08193 Bellaterra, Barcelona, Spain
[2] Department of Geology, University of Cincinnati, Cincinnati, OH 45221, USA

Received 4 December 2015; Revised 18 October 2016; Accepted 31 October 2016

*Correspondence to: Lucía Struth, Departament de Geologia, Universitat Autònoma de Barcelona, 08193 Bellaterra, Barcelona, Spain. E-mail: lucia.struth@gmail.com

ESPL
Earth Surface Processes and Landforms

ABSTRACT: Catchment-wide erosion rates were defined using ^{10}Be terrestrial cosmogenic nuclides for the Eastern Cordillera of the Colombian Andes to help determine the nature of drainage development and landscape evolution. The Eastern Cordillera, characterized by a smooth axial plateau bordered by steep flanks, has a mean erosion rate of 11 ± 1 mm/ka across the plateau and 70 ± 10 mm/ka on its flanks, with local high rates >400 mm/ka. The erosional contrast between the plateau and its flanks was produced by the increase in the orogen regional slope, derived from the progressive shortening and thickening of the Eastern Cordillera. The erosion rates together with digital topographic analysis show that the drainage network is dynamic and confirms the view that drainage divides in the Eastern Cordillera are migrating towards the interior of the mountain belt resulting in progressive drainage reorganization from longitudinal to transverse-dominated rivers and areal reduction of the Sabana de Bogotá plateau.

KEYWORDS: cosmogenic nuclides; erosion rates; drainage evolution; divide migration; eastern Cordillera of Colombia

Introduction

Rift inversion and/or crustal thickening result in dramatic topography and drainage network changes in mountain belts that are mainly controlled by major tectonic structures (Van der Beek *et al.*, 2002). The evolution and development of drainage systems in active orogens has attracted much attention recently, particularly with regard to transverse and longitudinal drainages, and drainage divides (Willett *et al.*, 2001, 2014; Pelletier, 2004; Bonnet, 2009; Castelltort *et al.*, 2012; Perron *et al.*, 2012; Goren *et al.*, 2014; Viaplana *et al.*, 2015). Clear examples of drainage rearrangement in relation to progressive mountain building have been described in the inverted rifts of the High Atlas of Morocco (Babault *et al.*, 2012) and Eastern Cordillera of Colombia (Babault *et al.*, 2013; Struth *et al.*, 2015). These studies highlight that drainage divides are dynamic features that progressively migrate and result in river capture events. Providing evidence for differential erosion rates on either side of a drainage divide adds much credence to developing and substantiating drainage evolution models for mountain belts (Willett *et al.*, 2014). As such, the side of a mountain belt with the greatest erosion will progressively migrate and capture drainages from the side with the least erosion. Theoretically, a dynamic drainage network will evolve towards a steady state, maintaining a steady drainage network and stationary drainage divides (Howard, 1965).

The Eastern Cordillera of Colombia is an example of an orogen with a dynamic drainage network (Babault *et al.*, 2013; Struth *et al.*, 2015). This N-S oriented orogenic belt has two topographic domains: (i) an axial zone with low relief associated with longitudinal rivers that have gentle gradients (the Sabana de Bogotá); and (ii) high-relief flanks with steeper transverse rivers. These domains are separated by what we refer to as the eastern and western main drainage divides. Recent studies have suggested that the increase of regional slopes due to progressive crustal thickening results in fluvial reorganization from longitudinal to transverse dominated drainages in the Eastern Cordillera (Babault *et al.*, 2013; Struth *et al.*, 2015). On the basis of a morphometric analysis, field observations and a summary of paleodrainage data, these studies conclude that drainage reorganization takes place by progressive drainage divide migration toward the axial zone of the orogen by a step-by-step series of river captures.

In this study, we build on the work of Struth *et al.* (2015) by using ^{10}Be terrestrial cosmogenic nuclides (TCNs) in fluvial sands to determine catchment-wide erosion rates for the Eastern Cordillera to investigate the contrasting erosion dynamics between the Sabana de Bogotá axial plateau and the flanks of the Eastern Cordillera. TCN analysis is combined with a comparative analysis of steepness index, specific stream power and the integral of the drainage area (χ values). We also

examine the role of local tectonics, lithology, and climate conditions as a control on drainage evolution.

Geological, morphological and climatological setting

The Eastern Cordillera of Colombia is an inverted continental rift in the northern Andes. The cordillera is composed of Precambrian-Paleozoic basement and a succession of Mesozoic and early Cenozoic sedimentary rocks within a doubly-verging thrust system (Julivert, 1970; Colletta *et al.*, 1990; Cooper *et al.*, 1995; Figure 1).

The Eastern Cordillera is flanked on both sides by lowlands composed of Cenozoic deposits, which infill the Magdalena Valley and the Llanos foreland basins that are at elevations of ~200–300 m above mean sea level (asl; Figure 1(A)). The flanks of the Eastern Cordillera are dominated by alternating Cretaceous sandstone and shale formations. Isolated Precambrian-Paleozoic basement massifs with low- and medium-grade metamorphic rocks (mainly phyllite and schist) are present in the Quetame and Floresta massifs (Segovia, 1965; Ulloa and Rodríguez, 1979; Ulloa and Rodríguez, 1982; Parra *et al.*, 2009a; Figure 1(A), (B)). The axial plateau of the Sabana de Bogotá is dominated by Cretaceous to Paleogene sandstone and shale that are deformed into open folds, whereas the Cordillera foothills have foreland facing thrust faults with

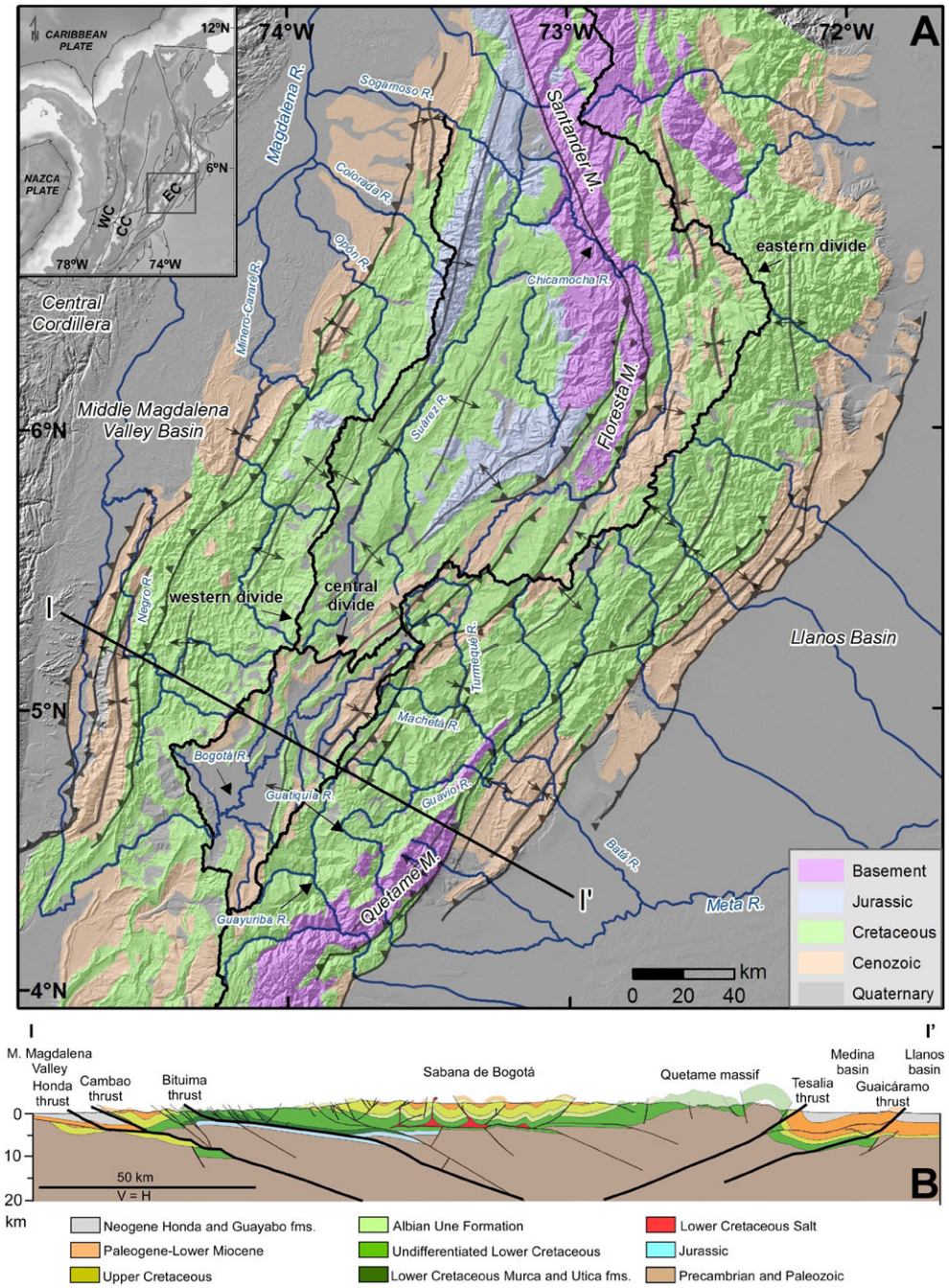

Figure 1. (A) Geology of the Eastern Cordillera of Colombia compiled from maps produced by Mora *et al.* (2010), Tesón *et al.* (2013) and unpublished maps of ICP-Ecopetrol. The fluvial network is represented with blue lines. Inset shows a map of the northern Andes showing the location of the Eastern (EC), Central (CC), and Western (WC) Cordilleras of Colombia. (B) Structural cross-section of the central part of the Eastern Cordillera (modified from Teixell *et al.*, 2015). Total shortening along this section is 82 km, consistent with values previously reported by Tesón *et al.* (2013) for the segment of the Eastern Cordillera covered by the map. [Colour figure can be viewed at wileyonlinelibrary.com]

large-displacement (Mora *et al.*, 2008 and references therein; Figure 1(B)). The local relief in the Sabana de Bogotá plateau is small because up to 600 m of unconformable Pliocene-Quaternary fluviolacustrine deposits partially fill the synclinal depressions (Tilatá and Sabana formations; Julivert, 1963; Andriessen *et al.*, 1993; Torres *et al.*, 2005). A moderate amount of orogenic shortening, 25 to 30%, across the Eastern Cordillera has been calculated along serial transects by Tesón *et al.* (2013) and Teixell *et al.* (2015).

There is a strong precipitation gradient across the western divide, whereas no precipitation gradient exists across the eastern divide (Figure 2). Precipitation is greatest ($> 3000\,\text{mm year}^{-1}$) near Charalá, in the eastern and western foothills and in the Quetame Massif.

Summary of the deformation and paleodrainage evolution of the Eastern Cordillera

Paleogene data show a western and southwestern source for the Central Cordillera foreland basin sediments, which currently include the early successions of deposits in the Magdalena Valley and Llanos basins, and the intervening Eastern Cordillera. Sediments moved NNE in the Central Cordillera foreland basin following the regional slope and the contemporaneous structures within the basin (Cooper *et al.*, 1995; Bayona *et al.*, 2008; Silva *et al.*, 2013). The drainage was longitudinal, parallel to the current Eastern Cordillera, following growing folds that thermochronological data show started to form during the Eocene (Parra *et al.*, 2009b; Mora *et al.*, 2010; Moreno *et al.*, 2011; Saylor *et al.*, 2011; Caballero *et al.*, 2013a, 2013b; Silva *et al.*, 2013).

The Magdalena and the Llanos basins became disconnected by the uplift of the Eastern Cordillera as deformation propagated eastward during the Late Oligocene to Early Miocene (Parra *et al.*, 2009b; Mora *et al.*, 2010). This is supported by provenance data indicating that the Eastern Cordillera developed into an effective topographic barrier that separated the Central Cordillera from the Llanos basin before the Mid to Late Miocene (Horton *et al.*, 2010). The axial Eastern Cordillera was likely a closed basin south of 6°N during the late Oligocene-Miocene (Silva *et al.*, 2013).

Base level started to rise in the Middle Magdalena Valley basin during the Late Oligocene to Mid Miocene, forcing its rivers to flow to the east, across the present location of the Eastern Cordillera, into the Llanos basin (Gómez *et al.*, 2005). The drainage in the Middle Magdalena Valley basin returned to flow to the north due to the continued uplift of the cordillera during the Mid-Late and Late Miocene. Since the Late

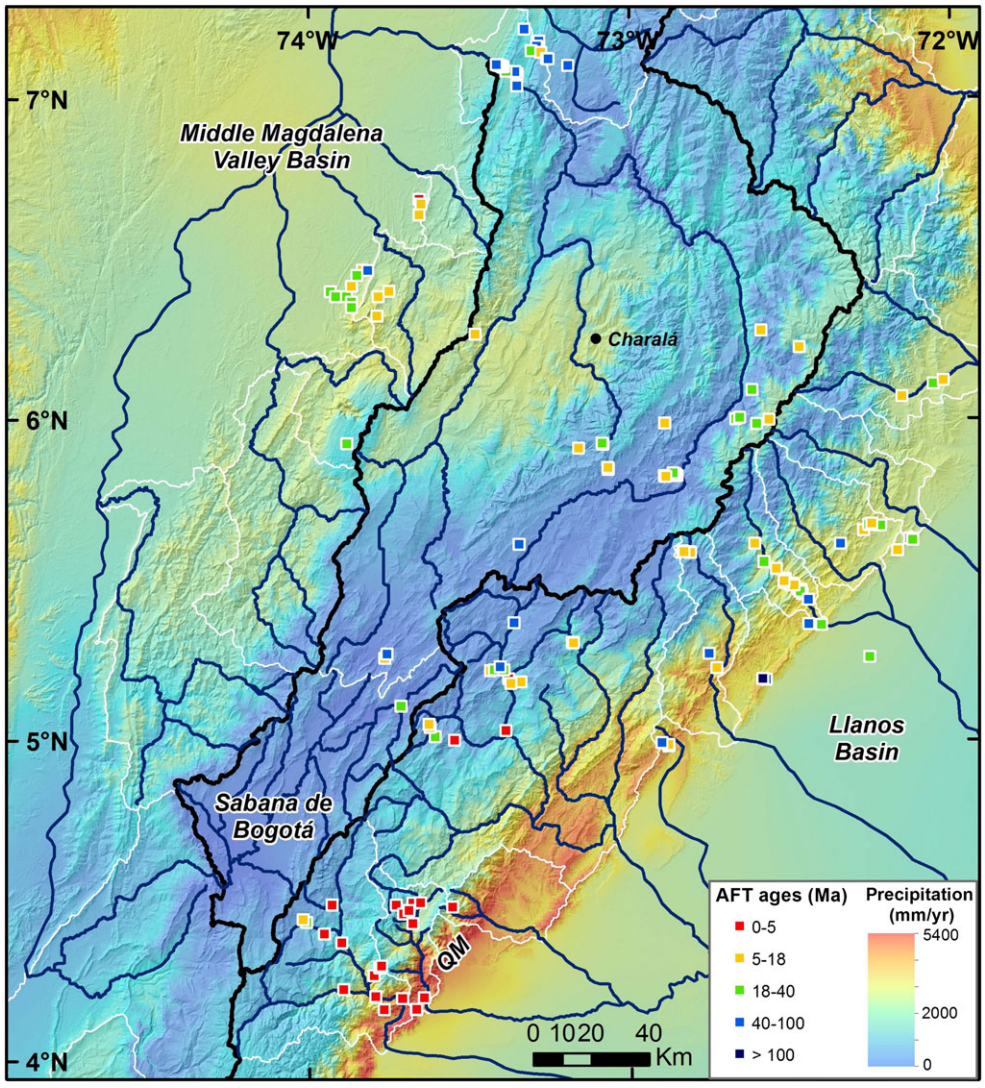

Figure 2. Mean annual precipitation data for the years 1998–2009 (after Bookhagen and Strecker, 2008) and Apatite Fission Track (AFT) data (after Mora *et al.*, 2008, 2010; Parra *et al.*, 2009a) in the Eastern Cordillera of Colombia. QM: Quetame Massif. White lines are the basin boundaries. [Colour figure can be viewed at wileyonlinelibrary.com]

Miocene, the paleoflow pattern in the eastern foreland of the Eastern Cordillera is characterized by a transverse drainage reflecting an eastward direction (Parra *et al.*, 2010) and providing sediments for the Llanos and Middle Magdalena Valley basins. Most external thrust sheets of the Cordillera are strongly deformed in recent times, and there are very young apatite fission track ages for the Quetame Massif along its eastern flank (0–3 Ma; Figure 3). This attests to strong exhumation across the Eastern Cordillera margins in the latest Neogene and Quaternary (Mora *et al.*, 2008) .

Struth *et al.* (2015) argue that the Eastern Cordillera is experiencing fluvial drainage network reorganization by drainage divide migration. Longitudinal drainages created in the early stages of drainage developed paralleling the structural grain of the growing tectonic orogen. The potential energy and power of transverse rivers was enhanced as the regional slope progressively increased during crustal thickening. This resulted in headward erosion causing drainage divide migration towards the Sabana plateau and capturing longitudinal streams: ultimately leading to drainage network reorganization.

Methods

Analysis of the digital drainage network

We used digital elevation model (DEM) SRTM90v4 that has a horizontal resolution of 90 m (Jarvis *et al.*, 2008) to analyze the drainage network for the Eastern Cordillera. The DEM was corrected in narrow areas that had low resolution using elevations from Instituto Geográfico Agustín Codazzi (IGAC) 1:100 000 topographic maps. Various geomorphic parameters provide information about erosion in channel networks and therefore information about the dynamism of the drainage. The most important parameters that we examine include stream power, steepness index and χ. We calculated these parameters to characterize the contrast between the topographic domains of the Sabana de Bogotá plateau and its flanks, and to identify which one best correlates with the TCN-derived erosion rates. We propose that a correlation between geomorphic parameters and TCN-derived erosion rates may allow a first estimation of erosion rates in areas devoid of TCN data.Stream power relates to the energy rate per unit distance along a river (Bagnold, 1966) and reflects the incision power of a river into bedrock under detachment-limited conditions (Howard and Kerby, 1983; Howard *et al.*, 1994; Whipple and Tucker, 1999; Kirby and Whipple, 2001). River incision is calculated according to the stream power model expressed as:

$$\partial z_{(x,t)}/\partial t = U_{(x,t)} - (KA^m S^n)_{(x,t)} \quad (1)$$

where U represents the bedrock uplift at x, K is the erosional efficiency, A is local drainage area and S is the channel slope. The positive exponents m and n describe the relative dependency of stream erosion rates on A and S.

Analysis of slope–area has frequently been used to reveal erosion trends in channel networks defined as steepness index or Ksn (Kirby and Whipple, 2001; Kirby, 2003; Snyder *et al.*, 2003; Wobus *et al.*, 2006; Dibiase *et al.*, 2010). However, local slope calculations undertaken for regions that have low DEM resolution such as the Eastern Cordillera of Colombia provide scattered and noisy results. For this reason, we calculate the channel slopes using the χ gradient referred to as Mx (Perron and Royden, 2013; Mudd *et al.*, 2014). To calculate Mx, we use the river profile elevation instead of the slope as the dependent variable, against χ as the independent variable. This approach produces more reliable results. We plot values of Mx, i.e. the slope in χ-elevation space (Mudd *et al.*, 2014), a parameter related to the ratio between erosion rate and erodibility (Perron and Royden, 2013), as a proxy to identify the distribution and magnitude of erosion. We defined the best concavity of the river profiles based on AICc-collinearity tests and χ-plots following the method of Mudd *et al.* (2014) to calculate Mx values. The AICc is a statistical method that selects a model that balances goodness of the fit against model complexity (Akaike Information Criterion, AICc; Akaike, 1974; Hurvich and Tsai,

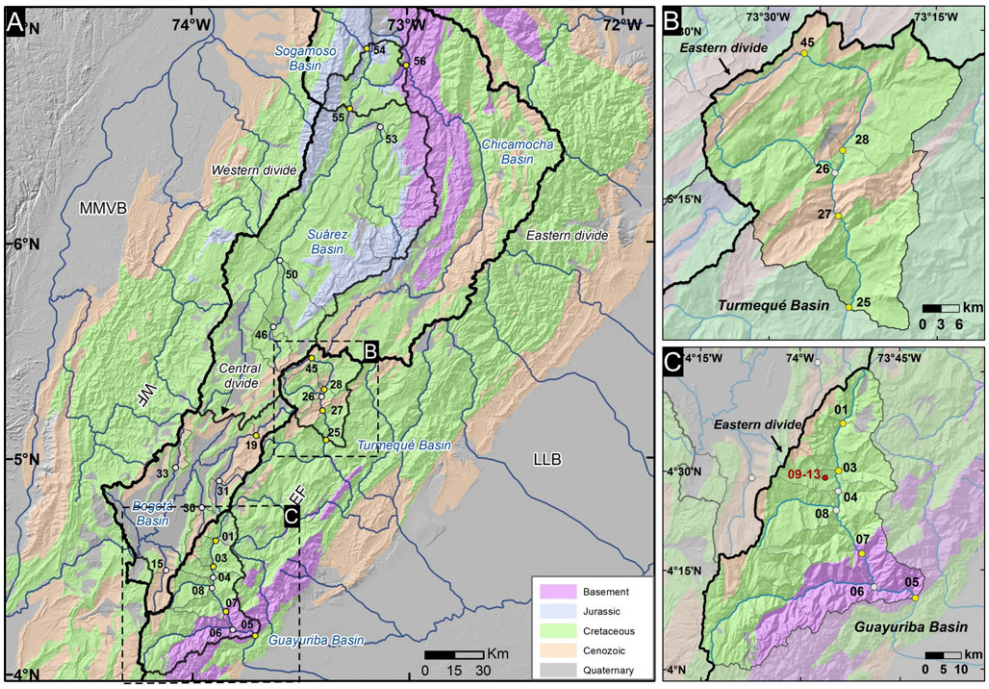

Figure 3. (A) Location of the fluvial sand samples from the trunk river (yellow) and tributaries (white) collected for ^{10}Be analysis. Detailed locations of sampling sites in (B) the Turmequé catchment and (C) for the Guayuriba catchment. Red point and label shows the location of the terrace boulder samples. LLB: Llanos Basin; MMVB: Middle Magdalena Valley Basin; EF: Eastern flank; WF: Western flank. [Colour figure can be viewed at wileyonlinelibrary.com]

1989; Burnham and Anderson, 2002). We extract the AICc-collinearity test and the χ plots for each basin based on iteration through a range of concavity values for the main channel and tributaries to define the best-fit concavity. The concavity with the minimum AICc value will be the best fitting one using this method. The mean calculated concavity for all the basins is 0.45 (see SD1). We compared the Mx values between different catchments by fixing the obtained concavity. Stream power theory predicts that river profiles will have a linear χ-plot and Mx proportional to the erosion rates, assuming, first, a steady-state condition, where rock uplift is balanced by erosion, and second, that erosion, erodibility and uplift are constant through time and space (Royden and Taylor Perron, 2013; Mudd *et al.*, 2014). In reality, U and K can be variable in space and time, which are dependent upon the tectonic and climatic history, and rock type. We calculated the concavity for all the basins following the method of Mudd *et al.* (2014) by extracting the steepness index, knickpoints and localize all the known active structures as well as highly erodible lithologies to solve this problem. In the case of stepped channel profiles associated with spatial or temporal changes in uplift rates, we used the colinearity test to identify the best concavity for each catchment (Mudd *et al.*, 2014). This technique allows the magnitude and distribution of the erosion rates to be identified.

We extract the χ-map following the method of Willett *et al.* (2014), and with a same base level determined by the elevation of the most external tectonic structures (300 m asl) and with a critical drainage area of 1 km^2 to extract information about the dynamics of the catchments. The main focus of this analysis rests on mapping differences in χ-coordinate values across drainage divides. Similar χ values on both sides of a drainage divide would suggest that the region is in equilibrium, while large differences in χ values across the drainage divide imply that river networks are in disequilibrium where divide migration or river capture is likely to occur (Willett *et al.*, 2014). Drainage divides generally migrate towards the higher χ values to achieve equilibrium, and hence, catchments with high values are prone to capture and may eventually disappear (Willett *et al.*, 2014). We extract the χ-map for the entire central segment of the Eastern Cordillera as a proxy for the dynamics of the drainage divides using a modified version of χ that makes a correction factor for the precipitation (Yang *et al.*, 2015) such that the χ value is defined by the following equation:

$$\chi(x) = \int_0^x \left(\frac{P_0 A_0}{A(x') P(x')} \right)^{\frac{m}{n}} dx' \quad (2)$$

where P_0 and A_0 are arbitrary scaling factors for the precipitation rate and drainage area, respectively, P is precipitation rate, A is the upstream drainage area and m and n are empirical and non-integer constants.

We also calculated an averaged specific stream power (SSP, Equation (3), Knighton, 1999) for each catchment following the method described in Godard *et al.* (2012) such that:

$$SSP = d\ g\ Ksn\ Q/W \quad (3)$$

where d is density, g is acceleration due to gravity, Ksn is the steepness index slope, Q is discharge and W is the channel width.

Terrestrial cosmogenic nuclides analysis

Sediment samples were collected for ^{10}Be TCN analysis to investigate erosional contrasts between the Sabana plateau and its flanks, including the main streams and major tributaries in the Guayuriba and Turmequé (representing the eastern flank of the Cordillera), Bogotá (Sabana de Bogotá plateau) and upper Suárez catchments. We followed the sampling methods of Carretier *et al.* (2015) who collected fluvial sand from the subcatchments to minimize issues associated with local lithologic variations. Rivers in the eastern flank and plateau have their headwaters on the same drainage divide, which allows us to make direct comparison between them. We also analyzed four ^{10}Be TCN samples in the lower Suárez and Chicamocha catchments (Figure 3, Table I) to examine the effect of a different vegetation cover, bedrock erodibility and climate. These four samples are not included in the comparative analysis between the plateau domain and the eastern flank.

Larger sampled catchment areas have higher likelihoods of including mixed fluvial signatures. In such cases, the erosion rate obtained may not be representative of all the reaches of that river, which may have experienced a diverse reorganization history.

Catchments including a relict flat area in their upper parts (Chicamocha, Suárez, Bogotá and Turmequé) reflect two different erosion regimes separated by a knickpoint (white stars in Figure 6). As such the upper part the catchment, above the mean knickpoints, should have lower erosion rates (related to lower relief, gentler slopes and lower Mx values) compared with those downstream. The Turmequé catchment illustrates this well, with an ancient plateau domain above the main knickpoint where the erosion rates are low (LUCN-45, 26) and higher erosion rates in its lower reaches (LUCN-25, 27, 28). We only sampled the upper part of the Bogotá catchment (LUCN-15, 19, 30, 31, 33) above the Tequendama Falls (see Figure 4 for location) to define the amount of erosion in it lowest erosion rate domain. We sampled its gently sloping upper reaches (LUCN-46, 50), and the steeper lower reaches below the knickpoint (LUCN-53, 55) in the Suárez catchment. Only one sample (LUCN-53) was collected in the Chicamocha valley catchment, which was located downstream of the main knickpoint.

We collected ~1 kg of sand for each sample. Catchment areas for each sample were large (>100 km^2) as recommended by Niemi *et al.* (2005) and Yanites *et al.* (2009) to provide a good representation of the ^{10}Be TCN inventory and the erosion rates. We use the erosion values obtained in the upstream reaches of the rivers that flank the Eastern Cordillera to compare the erosion rates between the rivers of the Sabana and the flanks of the cordillera. These flank rivers and those located in the Sabana, flow through alternating sandstone and shale formations in proportions that are similar in each different catchment. This similarity reduces the possibility of lithological biasing in sampling between our chosen catchments. The erosion rates determined by ^{10}Be reflect erosion on timescales of tens of thousands of years (Von Blanckenburg, 2005). In addition we sampled rivers across the western flank of the Eastern Cordillera, but we could not determine ^{10}Be concentrations in this region because we were unable to extract quartz from samples which were dominated by argillaceous sediment.

We also collected five quartzite samples for ^{10}Be TCN surface exposure dating from a well-preserved river terrace in the Guayuriba Basin (Figure 3(C), Table II). Such landforms are rare in our study area. Our sampled river terrace, which lies at ~406 m above the current stream, is not deformed, and it shows no evidence of erosion or landsliding. We collected ~500 g rock from the upper surfaces of fresh quartzite boulders inset into the river terrace. Topographic shielding was calculated by measuring the inclination to the skyline for every cardinal and intercardinal direction following the approach by Balco *et al.* (2008).

Table I. ^{10}Be sample details for rivers of the Eastern Cordillera including location, Be carrier weight and ^{10}Be concentrations measured. Carrier concentration was 1.023 ppm. See sample location in the map of Figure 3

Sample Number	Qz wt (g)	^{9}Be carrier weight (g)	Latitude (°N)	Longitude (°W)	Altitude (m)	^{10}Be/^{9}Be (10^{-15})	Number of Be-10 atoms (10^{3} at/g)
LUCN-01	30.4250	0.3504	4.6201	73.8926	2011	205.91 ± 83.26	162.11 ± 6.55
LUCN-03	23.7496	0.3506	4.5006	73.9040	1565	151.52 ± 9.19	152.90 ± 9.27
LUCN-04	30.7997	0.3516	4.4491	73.9048	1466	192.99 ± 9.29	150.61 ± 6.47
LUCN-05	29.6340	0.3514	4.1795	73.7116	719	28.07 ± 4.20	22.76 ± 3.40
LUCN-06	28.7791	0.3502	4.2077	73.8151	928	23.22 ± 2.35	19.31 ± 1.96
LUCN-07	30.3416	0.3504	4.2916	73.8455	1237	127.45 ± 8.80	100.61 ± 6.95
LUCN-08	30.0654	0.3510	4.4008	73.9100	1413	165.88 ± 6.76	132.38 ± 5.39
LUCN-15	30.3979	0.3496	4.4830	74.1217	2686	1225.00 ± 19.35	963.09 ± 15.21
LUCN-19	30.7441	0.3556	5.1087	73.7042	2631	1295.97 ± 27.81	1024.71 ± 21.99
LUCN-25	30.5609	0.3499	5.0873	73.3811	1349	213.23 ± 6.60	166.88 ± 5.16
LUCN-26	30.0070	0.3498	5.2879	73.4013	1953	852.14 ± 15.19	679.07 ± 12.11
LUCN-27	24.3370	0.3504	5.2237	73.3964	1797	200.61 ± 5.61	197.45 ± 5.52
LUCN-28	14.6113	0.3512	5.3216	73.3897	2020	135.99 ± 4.53	223.44 ± 7.44
LUCN-30	30.6254	0.3549	4.7742	73.9559	2516	855.50 ± 22.39	677.71 ± 17.73
LUCN-31	30.1409	0.3496	4.8982	73.8769	2607	3850.15 ± 49.01	3052.79 ± 38.86
LUCN-33	30.4318	0.3520	4.9595	74.0777	2621	1958.19 ± 52.60	1548.36 ± 41.59
LUCN-45	30.8061	0.3500	5.4666	73.4464	2762	3068.09 ± 85.63	2382.89 ± 66.50
LUCN-46	17.5983	0.3510	5.6125	73.6243	2113	944.56 ± 20.83	1287.87 ± 28.40
LUCN-50	21.3327	0.3498	5.9204	73.5932	1641	875.76 ± 17.04	981.67 ± 19.10
LUCN-53	29.7526	0.3502	6.5387	73.1259	1108	226.44 ± 5.57	182.20 ± 4.48
LUCN-54	21.8547	0.3506	6.9023	73.1873	354	52.17 ± 6.16	57.21 ± 6.76
LUCN-55	30.3494	0.3496	6.6232	73.2669	506	164.48 ± 4.95	129.52 ± 3.90
LUCN-56	29.8878	0.3495	6.8246	73.0055	555	63.06 ± 2.66	50.41 ± 2.12

Quartz isolation, purification, dissolution and preparation of BeO were undertaken in the geochronology laboratories at the University of Cincinnati following the methods of Kohl and Nishiizumi (1992) and described in detail in Dortch *et al.* (2009). All river sediment and river terrace boulder samples were sieved and crushed to 250–500 µm for the analysis. Samples were cleaned using HNO_3, HCl and HF and passed through a Frantz magnetic separator. Density separation was undertaken using lithium heteropolytungstate followed by an additional HF leach (Brown *et al.*, 1991; Kohl and Nishiizumi, 1992; Cerling and Craig, 1994). For each sample, 15–30 g of clean quartz grains was dissolved in HF and HNO_3 with 350 mg of ^{9}Be carrier. Beryllium was separated using anion and cation exchange columns. Beryllium hydroxide was obtained after fuming with $HClO_4$ acid and passing through anion and cation exchange columns (Bourlès, 1988; Brown *et al.*, 1992). The $Be(OH)_2$ was heated in an oven at 750 °C to form BeO and then loaded in steel target mixed with of Niobium (Nb) powder. ^{10}Be/^{9}Be ratios were measured by Accelerator Mass Spectrometry in the Purdue Rare Isotope Measurement (PRIME) Laboratory at Purdue University, Indiana, USA.

We took the standard approach and assumed that the amount of ^{9}Be in the prepared quartz was negligible. Sometimes this may not be the case, and quartz may contain some ^{9}Be. Such cases are rare, and almost invariably occur when quartz is derived from beryl-bearing granites or pegmatites, so that traces of Be and/or small amounts of beryl exist in the supposedly pure quartz sample, as documented in some areas of the Himalaya (Portenga *et al.*, 2015). However, pegmatites and beryl-bearing granites are not present in our study area. Any significant native ^{9}Be is therefore highly unlikely in our sampled quartz. If native ^{9}Be is present then denudation rates calculated from ^{10}Be concentrations will be overestimates, and the calculated erosion rates should be considered as apparent; however these rates can still be used for comparisons of variation across a region of similar lithologies (Corbett *et al.*, 2013; Portenga *et al.*, 2015).

To model catchment-wide erosion rates from ^{10}Be results we assumed that: (i) the sediment volume is proportional to the erosion rate, i.e. the catchment is close to steady-state; (ii) all the sediment collected at the sample locality was well mixed; (iii) the contribution of quartz was homogeneous in the catchment; (iv) that there is an isotopic equilibrium within the catchment, i.e. TCNs production in the catchment equals the transport of TCNs out of the catchment; and (v) the erosional timescale was significantly larger than the sediment transfer through the catchment (Lal and Arnold, 1985; Granger *et al.*, 1996; von Blanckenburg, 2005).

The corrected catchment-averaged production rates for ^{10}Be were calculated for each catchment using the SRTM90 digital elevation model following the method of Dortch *et al.* (2011) using MATLAB v. 2008 and the scaling factors provided in Lal (1991) and Stone (2000). With this method, the production rate for each pixel is calculated accounting for shielding to make an average for all the pixels in the catchment to obtain a spatially average production rate for the entire catchment (Lal, 1991). We use a ^{10}Be half-life of 1.36 ± 0.07 Ma (Nishiizumi *et al.*, 2007), the scaling model of Lal (1991) and Stone (2000) and a sea-level high-latitude production rate of 4.49 ± 0.39 ^{10}Be atoms/g SiO_2/a, for catchment erosion rates and river terrace dating.

^{10}Be ages for the river terrace samples were calculated using the CRONUS calculator (http://hess.ess.washington.edu/math/; Balco *et al.*, 2008). These ages will be minimum values and hence the resulting incision rates are maximum values. We are aware that the production rates and scaling models for ^{10}Be are being refined (Borchers *et al.*, 2016; Marrero *et al.*, 2016). Borchers *et al.* (2016) recently revised the production rate for sea level at high latitudes to 4.01 ^{10}Be atom/g SiO_2/a for the Lal (1991)/ Stone (2000) scaling model. However, we prefer to use the established scaling model and production rates in Balco *et al.* (2008) until there is community-wide agreement on the appropriate production and scaling. The new production rate results in an ~10% difference in the erosion rate from our preferred values.

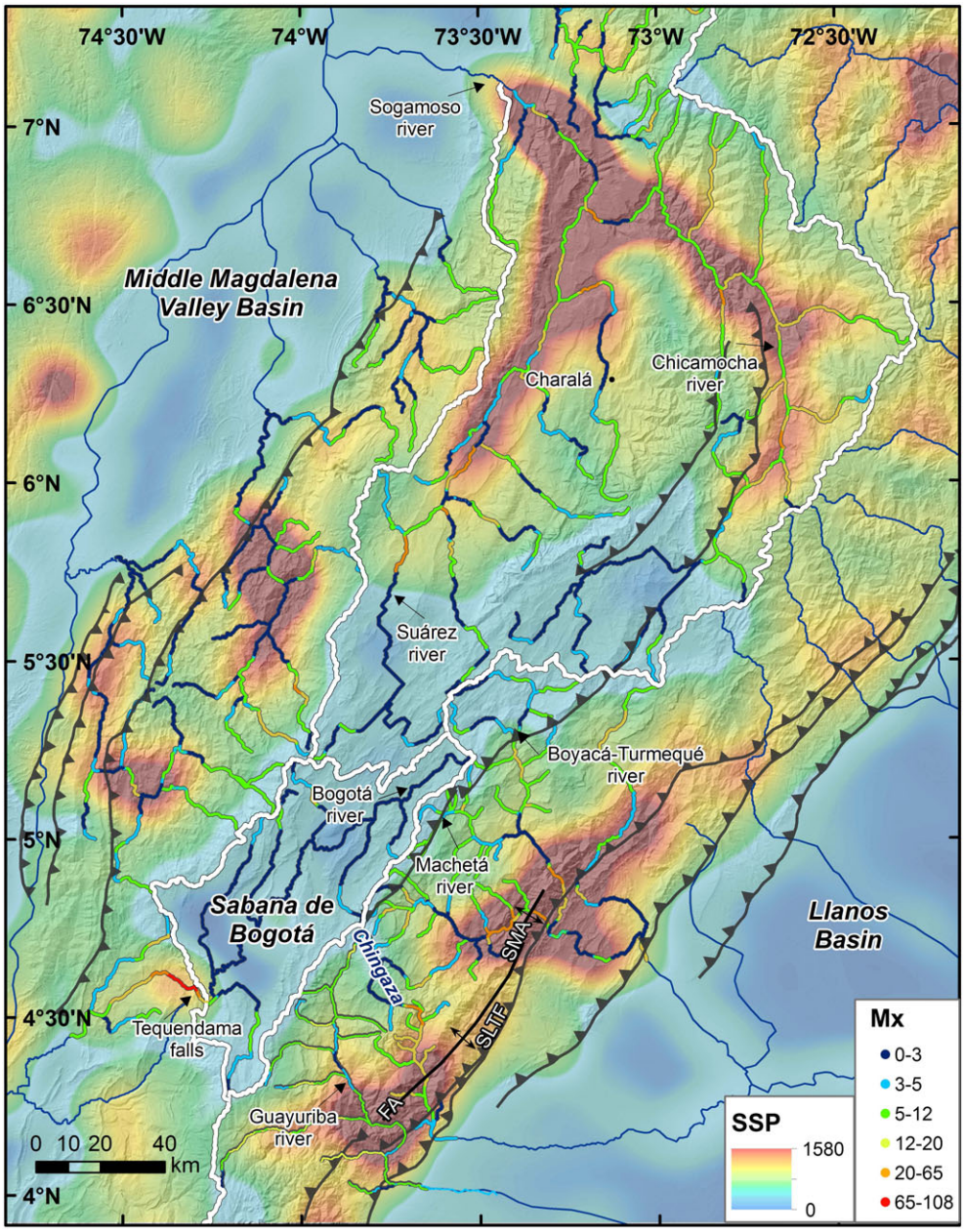

Figure 4. Distribution of specific stream power (SSP) values and Mx parameter (slope in χ-elevation plots) values for the analyzed rivers in the Eastern Cordillera of Colombia. White lines indicate the eastern and western drainage. χ plots are included in the Supplementary data. [Colour figure can be viewed at wileyonlinelibrary.com]

Results

Digital drainage analysis

The axial zone, which includes the Sabana de Bogotá and the southern part of the Sogamoso basin, is characterized by the lowest SSP values (Figure 4). In contrast, higher SSP values occur on the Eastern Cordillera flanks and in the northern areas of the Sogamoso basin, which argue for higher erosion rates than in the axial zone of the cordillera.

We extend the Mx map for the Eastern Cordillera of Colombia of Struth *et al.* (2015) that was limited to the area between 4°N and 5°30′N to between 4°N and 7°N. The Mx values have a similar distribution to the SSP, with higher values on the flanks and in the northern part of the Sogamoso basin than in the axial zone. The incision capacity is low (with low SSP) and values of Mx are also generally low (Mx = 0–3) in the Sabana plateau and the southern part of the Sogamoso basin. The eastern flank has average Mx values of between 5 and 12, with peak values between 20 and 27. Areas of recent tectonic uplift such as the Farallones and Santa Maria anticlines (Mora *et al.*, 2008), or where rivers dramatically increase gradient when they exit the high-elevation plains such as at the Tequendama Falls or at Chingaza, have the highest Mx values. The upper Sogamoso basin, with northward drainage, has low Mx values and is similar to those for Sabana de Bogotá. The Suárez basin has values between 4 and 7, while the Chicamocha basin has values between 6 and 12. Local high Mx values are associated with deeply incised stretches of the Suárez and Chicamocha rivers. Mx values in the higher parts of the western flank, bordering the divide, where rivers are of transverse type, range from ~5 to 12; Mx values decrease to between 1 and 4 in the lower part of the flank where the rivers are of longitudinal type. River profiles in χ space are shown in the Supplementary Data (SD2) and were partly published in Struth *et al.* (2015).

Table II. Description and ^{10}Be ages for the quartzite boulders on a river terrace in the Guayuriba valley with a carrier concentration of 1023 ppm. See sample location in the map of Figure 3(C)

Sample	Quartz mass (g)	^{9}Be carrier weight (g)	Latitude (°N)	Longitude (°W)	Altitude (m asl)	height/width/ breadth clast (cm)	Thickness (cm)	Shielding	^{10}Be/^{9}Be (10^{-15})	Number of Be-10 atoms (10^{3})	Exposure age (ka)	External uncertainty (ka)	Internal uncertainty (ka)
LUCN-09	29.765	0.3494	4.4659	73.9325	2133	30/60/80	2	1	3866.38 ± 90.64	310.52 ± 7.27	278	27	7
LUCN-10	30.936	0.3503	4.4672	73.9329	2135	40/40/60	4	1	3686.99 ± 69.19	285.39 ± 5.35	257	24	5
LUCN-11	28.108	0.3519	4.4675	73.9323	2131	40/180/150	3	1	7356.65 ± 116.02	627.81 ± 9.93	614	63	11
LUCN-12	29.743	0.3512	4.4675	73.9322	2129	40/200/400	2,5	1	8644.81 ± 146.22	697.80 ± 11.80	694	73	14
LUCN-13	28.115	0.3516	4.4675	73.9317	2125	50/150/120	3	1	7770.53 ± 134.31	664.29 ± 11.48	659	69	14

The χ values in the axial region of Sabana de Bogotá of the Eastern Cordillera (Figure 5) are higher than those for its flanks in the area of the drainage divide. A strong differentiation in χ values exists within the same domain: while the Sabana de Bogotá has low values near the central divide, the Sogamoso basin shows high values near the divide (Figure 5(B1)). In addition, χ values indicate disequilibrium between the Turmequé (with low values) and the Chicamocha (with higher values near the divide) basins (Figure 5(B2)).

Low SSP, Mx and precipitation, and high χ values in the headwaters of the rivers characterize the plateau, while high SSP, Mx and precipitation, and low χ values in the headwaters of the rivers characterize the flanks. In summary, the geomorphic indices clearly differentiate the plateau and flank domains within the Eastern Cordillera.

Landscape evolution rates

The large erosional contrast between the plateau and its flanks is evident from the variation in erosion rates derived from ^{10}Be analysis (Figure 6). The ^{10}Be analysis shows that for similar drainage areas, the erosion rates are lower in the Sabana de Bogotá plateau region (< 20 mm/ka) than on its flanks (>400 mm/ka (Table III). In more detail, the upper half of the Guayuriba catchment is eroding at a rate of ~75 mm/ka (samples LUCN-01, 03, 04, 08; Figure 6), whereas downstream the erosion rates are ~100, 479 and 670 mm/ka (LUCN-07, LUCN-05 and LUCN-06). Two samples (LUCN-05 and LUCN-06) show that erosion rates are an order of magnitude higher than the rest of the flank samples and provide the highest erosion rates (see discussion below). In the Turmequé catchment, the erosion rates increase progressively downstream from 5.5 mm/ka in the upper part of the catchment in the longitudinal tract (LUCN-45) to 15.7, 48, 53 and 59 mm/ka (LUCN-26, 28, 27 and 25) in the transverse tract (Figure 6).

The Sogamoso catchment drains the axial plateau of the Eastern Cordillera to the north, and is eroding at a rate of 167 mm/ka (LUCN-54; Figure 6). This catchment is divided into the Suárez catchment in the west and the Chicamocha catchment in the east, which are eroding at a rate of 64 and 228 mm/ka (LUCN-55 and 56), respectively. The upper part of the Suárez catchment is eroding at a rate of 8 and 10 mm/ka (LUCN-46 and 50). The erosion rate for the middle part of the Sogamoso catchment is 46 mm/ka (LUCN-53), and is similar to the erosion rate for the Suárez catchment.

TCN exposure ages for terrace boulders in the Guayuriba basin, assuming zero erosion and considered as minimum ages, range from 257 to 697 ka (Figure 7). However, the ages will be significantly older if we estimate an erosion rate using the oldest boulder age (LUCN-12) by applying the methods of Lal (1991). The erosion rate obtained from the oldest boulder is ~1 mm/ka and if we assume that all the samples erode at this rate, the initial ages with zero erosion will increase by up 50% for ages up to ~700 ka. However, since we sampled large boulders with no apparent weathering, we can assume that a correction factor for erosion is not really necessary for our ages.

The ranges of ages show significant scatter, but the three oldest samples (LUCN-11 to LUCN-13) clustered particular well given their antiquity, with a mean age of 656 ± 69 ka. We argue that the two youngest ages probably reflect exhumation of the boulders from the terrace and so we do not use those ages in our incision rate calculation. Given the mean elevation of the three oldest samples is 2129 ± 3 m asl and the elevation in the adjacent valley is ~1723 m asl, we use a height difference of 406 ± 5 m to calculate an incision rate of ~62 mm/ka.

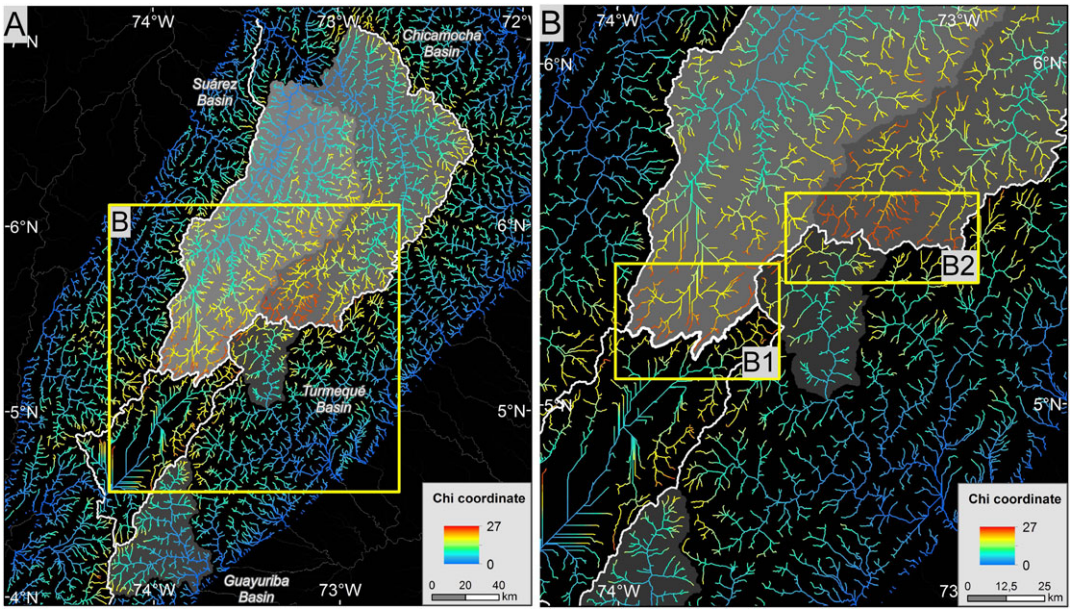

Figure 5. χ values for the river networks in the Eastern Cordillera (for a m/n ratio of 0.45). B1 and B2 areas are described in the main text. Discontinuities in χ across divides indicate that the network is not in geometric equilibrium. The waters divides generally move in the direction of higher chi. [Colour figure can be viewed at wileyonlinelibrary.com]

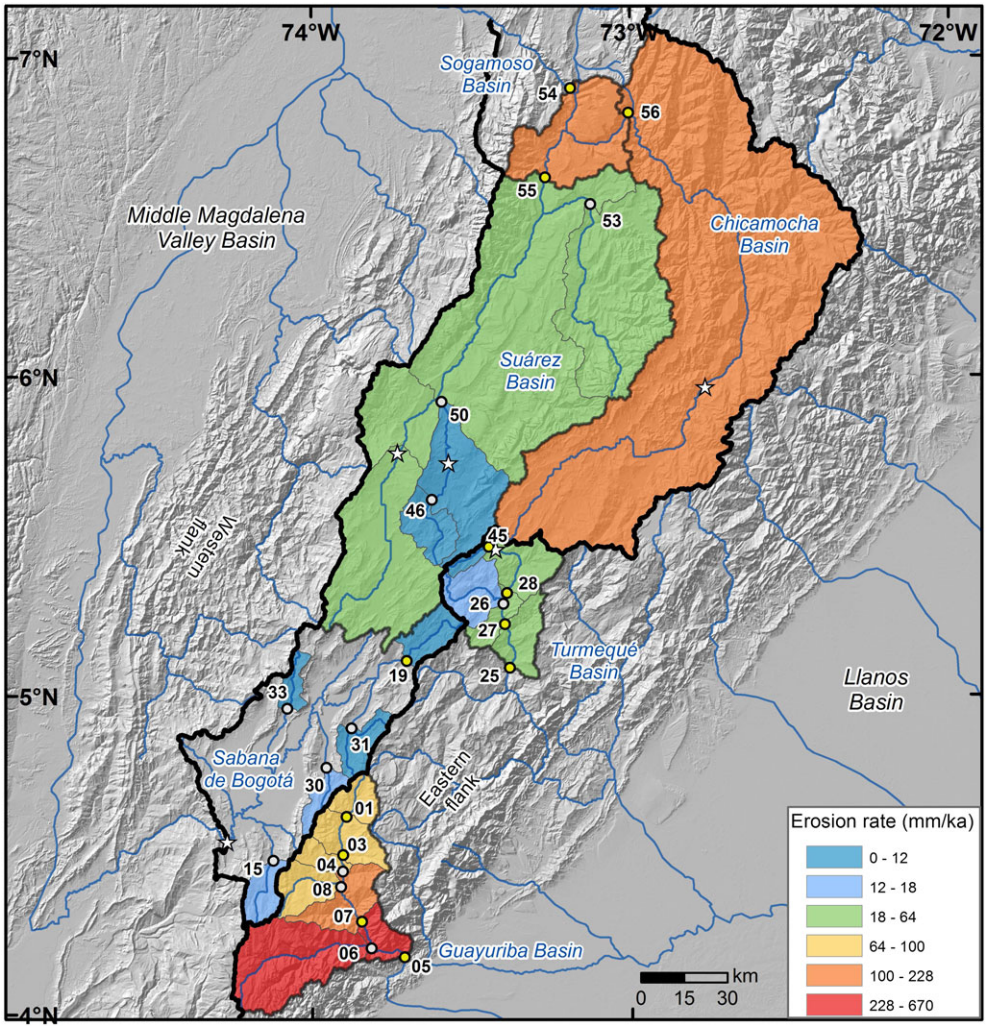

Figure 6. Erosion rates calculated for selected Eastern Cordillera catchments by ^{10}Be TCN analysis of river sediments. Points and numbers indicate fluvial sample with prefix LUCN-XX, yellow for the trunk samples and white for the tributaries. White stars indicate the location of the plateau capture knickpoint in the Suárez, Chicamocha and Bogotá rivers. The main drainage divides are indicated by thick black lines. [Colour figure can be viewed at wileyonlinelibrary.com]

Table III. ^{10}Be TCN data for samples of the Eastern Cordillera. Also shown are rainfall, SSP and Mx values for each sampled basin.

Sample	Sample catchment area (km^2)	Avg. elevation (m)	Standard deviation (m)	MATLAB ^{10}Be P-rate	^{10}Be concentration (10^5 at/g)	Attenuation length (m)	Erosion rate (mm/ka)	Rainfall rate (mm/a)	SSP (GJ/m2/a)	Mx
LUCN-01	200.5	3071	397	21.3 ± 2.8	1.621 ± 0.065	0.6	79.2 ± 10.9	1331 ± 112	39.28 ± 5.08	7.87 ± 2.77
LUCN-03	526.3	2808	512	18.6 ± 2.4	1.529 ± 0.092	0.6	73.3 ± 10.6	1337 ± 177	51.59 ± 14.28	8.18 ± 2.18
LUCN-04	658.8	2760	531	18.2 ± 2.4	1.506 ± 0.064	0.6	72.6 ± 10.1	1318 ± 186	53.56 ± 16.34	8.43 ± 2.45
LUCN-05	2559.7	2726	701	18.1 ± 2.4	0.227 ± 0.034	0.6	479.4 ± 95.8	1678 ± 684	99.71 ± 63.88	9.28 ± 2.93
LUCN-06	1010.1	3054	685	21.5 ± 2.8	0.193 ± 0.019	0.6	670.7 ± 111.9	1648 ± 453	106.27 ± 53.89	9.81 ± 3.33
LUCN-07	1334.5	2610	560	16.7 ± 2.2	1.006 ± 0.069	0.6	100.1 ± 14.9	1445 ± 327	71.90 ± 35.86	8.64 ± 2.61
LUCN-08	293.1	2645	526	17.0 ± 2.2	1.323 ± 0.053	0.6	77.5 ± 10.7	1280 ± 192	57.60 ± 20.30	9.72 ± 2.51
LUCN-15	239.9	3352	278	24.7 ± 3.2	9.630 ± 0.152	0.6	15.4 ± 2.0	1202 ± 149	33.33 ± 2.16	5.08 ± 1.57
LUCN-19	265.3	2910	189	19.4 ± 2.5	10.247 ± 0.219	0.6	11.4 ± 1.5	923 ± 151	17.62 ± 3.77	2.44 ± 1.46
LUCN-25	1291.2	2605	394	16.5 ± 2.1	1.668 ± 0.051	0.6	59.5 ± 8.0	1094 ± 207	39.53 ± 18.37	5.32 ± 2.37
LUCN-26	345.6	2742	286	17.7 ± 2.3	6.790 ± 0.121	0.6	15.7 ± 2.0	982 ± 81	30.12 ± 8.77	3.73 ± 1.42
LUCN-27	977.2	2708	325	17.4 ± 2.3	1.974 ± 0.055	0.6	53.1 ± 7.1	1008 ± 98	31.78 ± 11.81	4.66 ± 1.85
LUCN-28	459.9	2749	325	17.9 ± 2.3	2.234 ± 0.074	0.6	48.1 ± 6.5	997 ± 98	25.94 ± 5.48	4.82 ± 1.59
LUCN-30	162.5	3010	200	20.5 ± 2.7	6.777 ± 0.177	0.6	18.2 ± 2.4	1045 ± 110	21.58 ± 6.12	6.48 ± 1.1
LUCN-31	244.6	2961	264	20.0 ± 2.6	30.527 ± 0.388	0.6	3.9 ± 0.5	1152 ± 180	19.26 ± 5.72	3.35 ± 1.43
LUCN-33	134.9	3072	250	21.2 ± 2.8	15.483 ± 0.415	0.6	8.3 ± 1.1	1054 ± 125	19.54 ± 2.98	3.12 ± 1.83
LUCN-45	64.9	3119	174	21.8 ± 2.8	23.828 ± 0.665	0.6	5.5 ± 0.7	1097 ± 133	20.52 ± 0.57	2.8 ± 0.57
LUCN-46	313.4	2592	305	16.3 ± 2.1	12.878 ± 0.284	0.6	7.6 ± 1.0	1072 ± 90	17.46 ± 3.02	1.89 ± 1.28
LUCN-50	1185.8	2545	401	16.0 ± 2.1	9.816 ± 0.191	0.6	9.8 ± 1.3	1221.61 ± 268.18	34.50 ± 22.07	3.58 ± 3.07
LUCN-53	2083.3	2251	738	14.0 ± 1.8	1.822 ± 0.044	0.6	46.4 ± 6.2	2101.65 ± 577.49	80.70 ± 29.59	5.72 ± 2.12
LUCN-54	20153.1	2441	777	15.9 ± 2.1	0.572 ± 0.067	0.6	167.1 ± 29.6	1618.68 ± 630.75	95.79 ± 91.41	7.01 ± 4.78
LUCN-55	9789.2	2232	650	13.7 ± 1.8	1.295 ± 0.039	0.6	63.8 ± 8.6	1889.11 ± 716.5	78.81 ± 60.33	5.92 ± 4.78
LUCN-56	9307.1	2792	720	19.1 ± 2.5	0.504 ± 0.021	0.6	228.4 ± 31.7	1360.68 ± 399.12	86.02 ± 59.49	8.13 ± 4.72

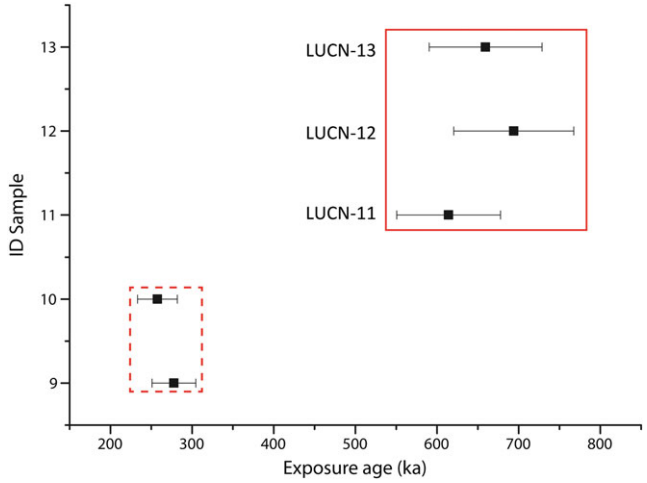

Figure 7. ^{10}Be age for the terrace boulders. LUCN-09 and 10 show an exposure age of 267 ± 16 ka (dashed line). LUCN-11, 12 and 13 mark an older mean exposure age of 656 ± 69 ka. [Colour figure can be viewed at wileyonlinelibrary.com]

This is comparable with the catchment-averaged erosion rates calculated from river sediment from the flank streams.

Discussion

Calculated erosion rates for the Eastern Cordillera using ^{10}Be and values of SSP, Mx and χ show clear erosional contrasts between the axial plateau and its flanks. Intra-domain and intra-basin differences are also apparent between regions.

Drainage network dynamics

Rivers across the flanks of the Eastern Cordillera need more erosion capacity than the longitudinal rivers in the Sabana plateau for river capture to occur (Struth *et al.*, 2015). Higher erosion rates along the flanks of the Eastern Cordillera (>50 mm/ka) compared with the Sabana plateau (<20 mm/ka) suggests that retreat of the main divides and capture of the longitudinal plateau rivers by the transverse flank rivers is occurring. The Guayuriba and the Bogotá catchments provide examples of flank catchments with a drainage area of 200 km^2 yielding an erosion rate of 79 mm/ka (LUCN-01), whereas the plateau catchments with comparable drainage areas of 163 and 245 km^2 yield erosion rates of 18 (LUCN-30) and 4 mm/ka (LUCN-31), respectively (Figure 6). For a plateau catchment with an area of 240 km^2, an erosion rate of 15 mm/ka (LUCN-15) was determined, which is lower than a similar size catchment (293 km^2) on the eastern flank that has an erosion rate of 77 mm/ka (LUCN-08). Comparisons between the Turmequé and Sogamoso catchments also illustrate this contrast; sampled catchments for Suárez, with areas of 313 and 1186 km^2, provided rates of 7 and 10 mm/ka (LUCN-46 and 50). This is markedly different from the Turmequé flank samples from drainage areas of 460 and 1291 km^2 that have higher erosion rates of 48 and 59 mm/ka (LUCN-28 and 25), respectively. These results confirm that the main drainage divides in the Eastern Cordillera will migrate towards the axial plateau because rivers in the flanks have more energy (indicted by SSP values) and erosion capacity (reflected in the Mx values).

A special case is illustrated by comparing the Sabana catchment where sample LUCN-19 was collected (with a drainage area of 265 km^2 and an erosion rate of 11 mm/ka) with the Turmequé catchment flank where samples LUCN-45 (65 km^2, 6 mm/ka) and LUCN-26 (346 km^2, 15 mm/ka) were collected. This sampled area round these samples was interpreted by Struth *et al.* (2015) as a drainage capture zone on the basis of topography, featuring a depressed topographic profile and a mapped reentrant toward the west of the main divide, and of the occurrence of knickpoints upstream of a fluvial elbow (sharp change in the river channel direction) in map view. Similar erosion rates on both sides of the drainage divide in the Turmequé area argue in favor of drainage capture. In addition, the χ-values map shows that the upper part of the Turmequé catchment was part of the plateau area in the past and is now incorporated into the flank domain (Figure 5(B1)).

As documented by Struth *et al.* (2015), the Eastern Cordillera of Colombia has clear geomorphic differences between its flanks and axial zone, which includes the Sabana de Bogotá and the southern low-relief part of the upper Sogamoso catchment. Comparison of the geomorphic indices and the erosion rate results with the drainage divide features argue for capture processes. This confirms the view of Struth *et al.* (2015) and Babault *et al.* (2013) who proposed drainage divide migration and a longitudinal to transverse drainage rearrangement in the Eastern Cordillera.

Correlation of erosion rates with Mx values (Figure 9) is stronger than with the SSP (Figure 8). The SSP is, at a first order, a function of precipitation, slope and drainage area. Calculation of the SSP from a series of raster measurements and the low-resolution data of the DEM or the precipitation provide equivocal results. Mx is solely a function of the elevation and distance of the river profile, providing a more realistic value to describe the steepness of the river reaches.

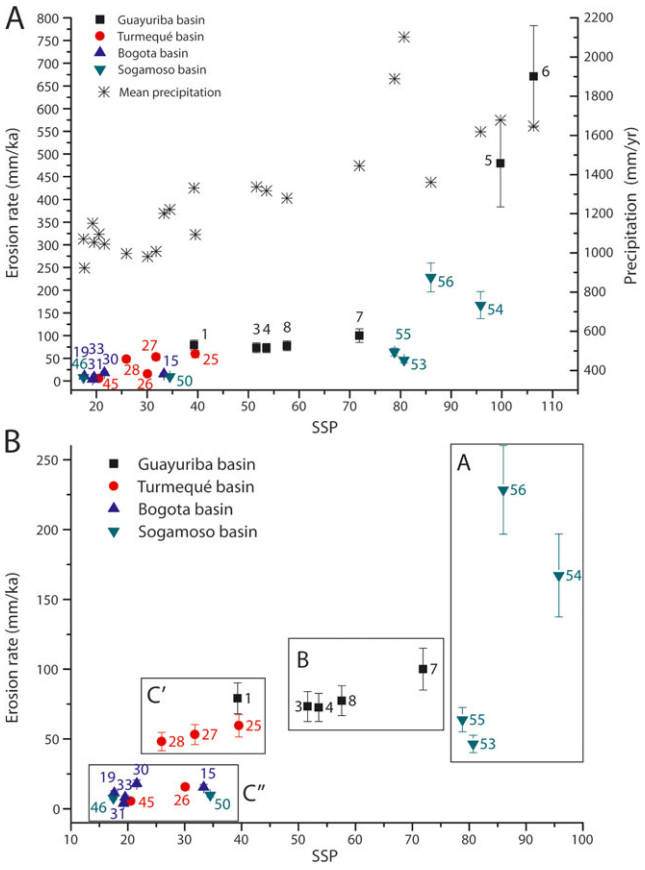

Figure 8. (A) Plots of erosion rate (mm/ka) vs. mean SSP value and precipitation for each sample and basin analyzed in this study. (B) Rescaling of the main graph for better comparison of the individual trends observed for the SSP values, excluding the two highest rate samples, LUCN-05 and 06 (see discussion for the A-C″ groups). [Colour figure can be viewed at wileyonlinelibrary.com]

Calibration of geomorphic parameters

The links between erosion rates and SSP or Mx have been examined in previous studies (Kirby and Whipple, 2012; Perron and Royden, 2013; Safran *et al.*, 2005; Bookhagen and Strecker, 2012). Our data reveal high erosion rates derived from samples located on the flanks of the Eastern Cordillera (which show high SSP) and in the northern parts of the Sogamoso basin, and low rates for the axial plateau (Sabana de Bogotá, upper part of Turmequé basin and southern part of the Sogamoso basin).

Geomorphic indices cluster into four groups (A, B, and C in Figure 8(B)). Group A comprises Sogamoso catchment samples from the most incised northern part of that catchment (LUCN-53, 54, 55, 56). Group B is associated with flanks that are characterized by high relief, and group C includes the lowest relief area samples. Group C is subdivided into C′, including samples with flank characteristics but with lower relief (LUCN-25, 27, 28 and 01), and C″, with plateau characteristics (LUCN-19, 26, 31, 33, 45, 46, 50).

Erosion rates and the catchment-wide average Mx values correlate positively (Figure 9). Despite the four samples having different lithologies, climate and uplift conditions (dashed box in Figure 9), a polynomic equation is defined for the rest of samples (Trend A = red line in Figure 9). Trend A reflects samples with similar lithologies and in areas of similar precipitation and uplift. This trend is linear and can be expressed in the form:

$$E = a_1 \cdot Mx \quad (4)$$

where a_1 is 12.28.

Equation (4) might be used as a proxy for estimating erosion rates when TCN data are not available or cannot be obtained. However, the applicability of Equation (4) for the shale-rich western flank of the Eastern Cordillera of Colombia might be problematic. This is because the western flank is a shale-dominated area with more erodible rocks while the eastern flank is composed of alternating sandstone and shale formations that are more resistant; hence application of Equation (4) for the western side will provide underestimates of the erosion rates.

Local climatic, bedrock and tectonic effects

Classifying our samples into four groups, according to their erosion rates, provides an additional means of differentiating between the axial plateau and the cordillera flanks (Figure 10):

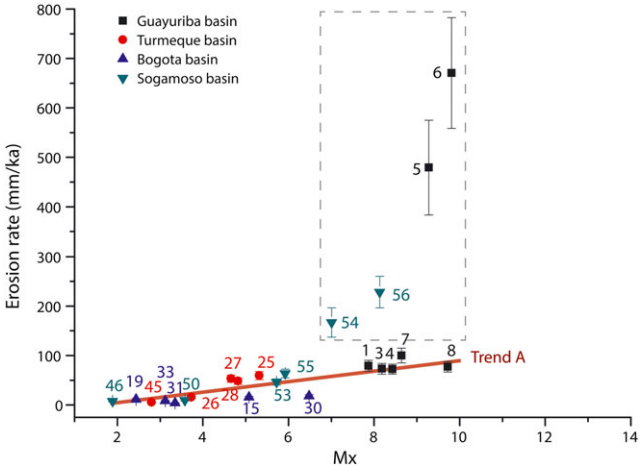

Figure 9. Erosion rates (mm/ka) plotted against the mean Mx value for each sample and basin analyzed (see discussion for the samples included in Trend A). [Colour figure can be viewed at wileyonlinelibrary.com]

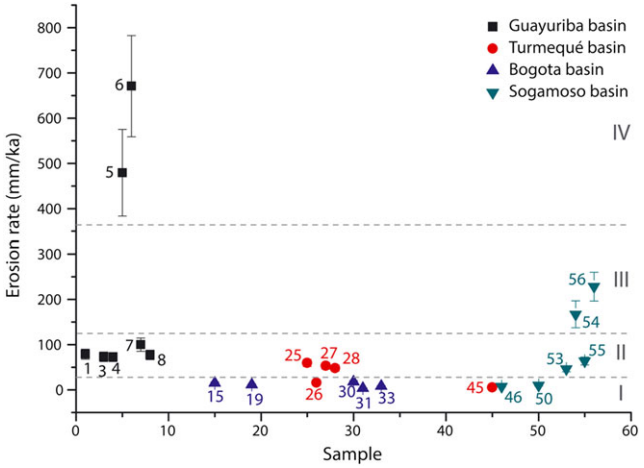

Figure 10. Erosion rates (mm/ka) for each sample. Sample numbers correspond to the ending number of the LUCN-XX numeration. [Colour figure can be viewed at wileyonlinelibrary.com]

Group I represents the plateau domain, with the lower erosion rate values (<20 mm/ka). This area is a relatively little tectonically deformed belt of the cordillera (Mora *et al.*, 2008, Teixell *et al.* 2015), and is associated with longitudinal, structure-controlled fluvial drainage. Samples LUCN-26 and 45 are not located on the plateau, but the low relief of these catchments and the longitudinal trend of the rivers suggest they were part of the plateau in the past.

Group II samples represent an incised domain, including some of the samples located in the flanks and in the Sogamoso catchment (Suárez River). The samples located in this group are from high-energy rivers that are transverse to the chain, and cut across the structural grain.

Group III includes only two samples, LUCN-54 (167 mm/ka, Sogamoso river) and LUCN-56 (228 mm/ka, Chicamocha river). The difference between erosion rates for these samples and the adjacent catchments, 46 mm/ka (LUCN-53) compared with 64 mm/ka (LUCN-55), correlates with a difference in climate, vegetation cover and rock strength. Basement composed of low- and medium-grade metamorphic rocks is exposed in the upper and medium part of the Chicamocha basin (LUCN-56), and the region has little vegetation. In contrast, the Suárez river basin (LUCN-55) mainly traverses alternating Cretaceous sandstone and shale formations. In terms of erodibility, and according to Castro (1992) and González and Jiménez (2015), basement rocks are more erodible than Cretaceous sedimentary rocks. Moreover, erosion is enhanced because of the lack of vegetation cover in the upper and middle part of the Chicamocha basin. The Chicamocha valley has an arid microclimate unlike any other part of the Eastern Cordillera. The valley is very narrow and the obtained data (Figure 2) from the few pluviometer stations do not reflect the real conditions inside it, resulting in overestimates of precipitation. The Cocuy-Santander massif to the east and the Floresta massif to the west bound the Chicamoca valley (Figure 1). These massifs form an orographic barrier and result in a rain shadow zone within the Chicamocha valley. The Chicamocha river is characterized by a very high mean Mx (~ 8.13) with steep hillslopes and an erosion rate of 228 ± 32 mm/ka. The Suárez river (sample LUCN-54) mainly flows across Cretaceous formations and Mx values are low (~ 5.92), with an erosion rate of 63.8 ± 8.6 mm/ka. The Chicamocha catchment, with higher erosion rate, has lower precipitation than the Suárez catchment, which is similar to the Sabana de Bogotá. If high precipitation results in large erosion rates, then higher erosion rates would be expected in the wetter Suárez catchment than in the Chicamocha catchment; but this is not the case. We

propose that the high erosion rate in the Chicamocha valley is related to the local 'semiarid' conditions, low vegetation cover and more erodible bedrock, all of which will enhance the erosion capacity. We underline the importance of rock type in determining the magnitude of the erosion within similar topographic domains, as shown in other studies in dynamic settings where higher denudation rates that have been related to high erodibility of the rocks (Salgado *et al.*, 2008; Chadwick *et al.*, 2013; Bierman *et al.*, 2014; Pupim *et al.*, 2015). Safran *et al.* (2005) showed that the rock type might play a secondary non-dominating role in catchment-averaged erosion rates in the Bolivian Andes, where high erosion rates were found in catchments that have weak or resistant bedrock. That work proposed that uplift had a first-order effect on erosion rates, with rock type playing a second-order effect, and climate had little if any influence on erosion. However, rock type, vegetative cover and climate have a first-order effect on erosion in the Eastern Cordillera of Colombia.

Group IV is composed only by two samples, LUCN-05 (479 mm/ka) and LUCN-06 (670 mm/ka), which yielded strongly different erosion rates compared with the rest of the Guayuriba catchment samples, as for example the sample LUCN-03 with an erosion of 73 mm/ka. Group IV samples are located in the Quetame basement massif (that is easily eroded), characterized by higher precipitation values and younger exhumation ages (Mora *et al.*, 2008, 2010; Parra *et al.*, 2009a) than in the upper part of the catchment, as indicated by greater erosion and incision (see Figure 2). The combination of greater precipitation and exhumation defines a closed feedback erosive cycle, in accordance with the high erosion rates determined for this area.

Up to 150 mm/ka differences in erosion rates are observed in catchments within the same topographic domain (Figure 6). The difference between the Suárez (64 ± 9 mm/ka) and Chicamocha (228 ± 32 mm/ka) catchments is probably due to a combination of precipitation and lithologic effects. Erosion rates in the eastern flank catchments are not homogeneous, as is, reflected by the Guayuriba basin showing higher erosion rates, relief and incision values than the Turmequé catchment (Figures 2 and 11).

The contrast in erosion rates described above argues for different fluvial dynamics between the Guayuriba and Turmequé catchments. The upper part of the Turmequé catchment has clearly been captured, as suggested by geomorphic analysis in Struth *et al.* (2015). Our current work adds new analysis using the χ and SSP values suggesting a rearrangement of the axial longitudinal drainage by transverse rivers that traverse the flanks of the cordillera. The disequilibrium in the χ values

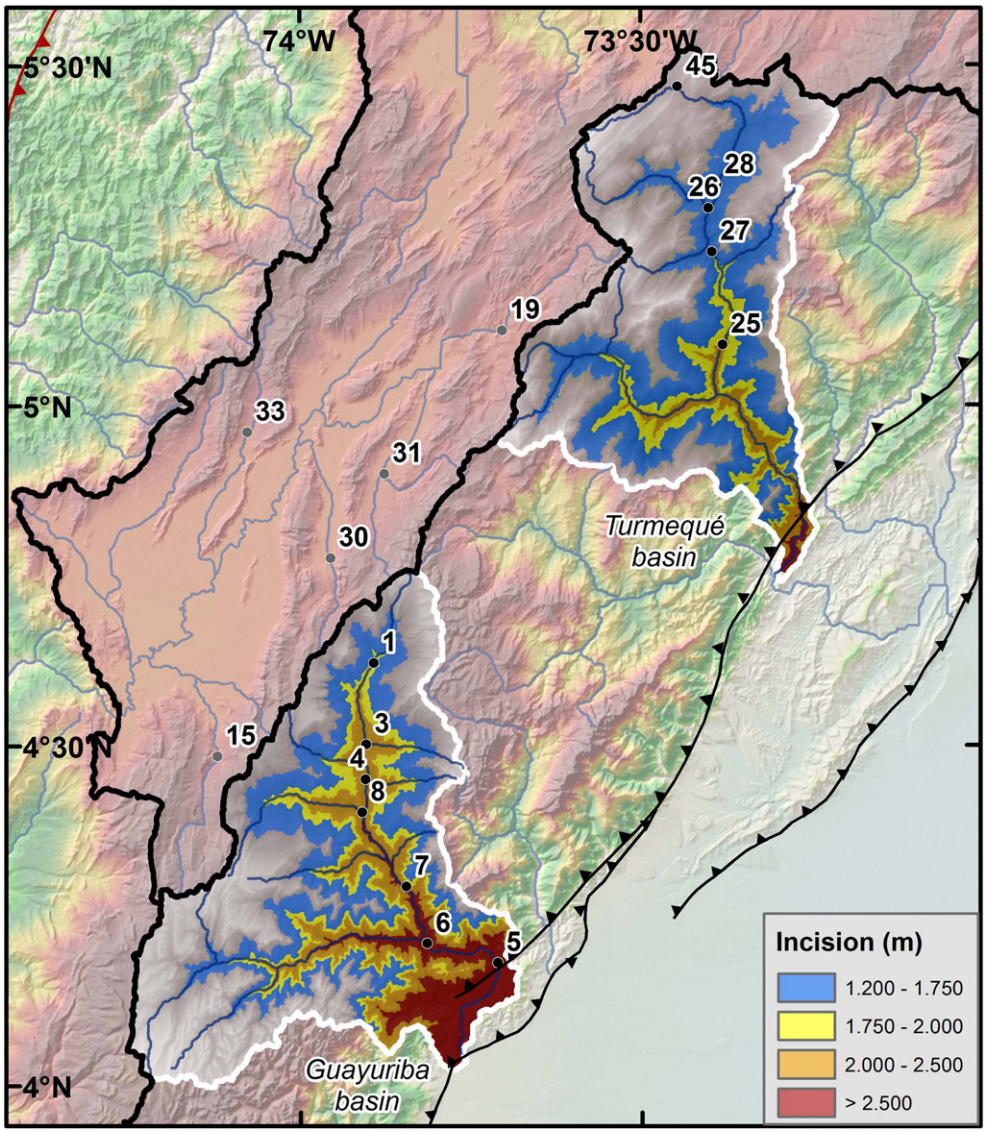

Figure 11. Incision values for the Guayuriba (south) and Turmequé (north) basins calculated by the subtraction of the DEM elevation of the valley floors from the maximum elevation of the lateral ridges. Numbered points indicate samples. Note higher values of incision in the Guayuriba basin compared with the Turmequé basin. [Colour figure can be viewed at wileyonlinelibrary.com]

for both sides of the eastern and central divides suggests drainage divide migration toward the inner part of the plateau's interior and to the north, respectively. This drainage divide migration is more evident for the Turmequé catchment than for the Guayuriba catchment. This supports the view of Struth *et al.* (2015) who suggested that the Turmequé area was a captured reentrant.

The different geomorphic characteristics of the eastern drainage divide and between the two catchments are interpreted as the result of the competition between uplift and erosion. In the Guayuriba catchment, the erosive potential results from the high contrast between slopes during mountain building and the active tectonics in the basin that has young thermochronologic ages (Mora *et al.*, 2008, 2010; Parra *et al.*, 2009a; Figure 2), arguing for high erosive potential to compensate the high uplift in the foothills of the flanks. In this way, the upstream propagation of erosion and then, the capture and divide migration is less probable in a catchment with low exhumation such as the Turmequé catchment.

Struth *et al.* (2015) interpret the different river dynamics between the flanks and the axial plateau of the Eastern Cordillera as a product of mountain building and drainage development. As such there was progressive increase in the regional slope caused by the accumulation of crustal shortening and thickening, as documented for the Moroccan High Atlas (Babault *et al.*, 2012). Essentially, the contrast in regional slopes results in different erosion rates and topographic dynamics across the Eastern Cordillera. Variations in local precipitation, tectonics and bedrock within a basin may also influence its erosion dynamics, and may have played a secondary role in the dynamism of divide migration and landscape evolution.

Conclusions

A smooth axial plateau flanked by steep topographic belts characterizes the Eastern Cordillera of Colombia. New ^{10}Be TCN data reveal high erosion rates for catchments along the high-relief flanks of the Eastern Cordillera, with a mean value of 70 ± 10 mm/ka (exceeding 400 mm/ka in some catchments). In contrast, the mean erosion rate is 11 ± 1 mm/ka for the low-relief axial plateau. This argues for erosional contrasts between the two domains and a migration towards the plateau of the N-S oriented plateau–flanks drainage divides. Results of digital morphometric analysis, including specific stream power, steepness index and χ values confirm the view that the drainage divide in the Eastern Cordillera is asymmetric and is moving by processes of river capture. Drainage reorganization from longitudinal to transverse, dominated by means of a series of river capture events, will lead to a progressive reduction of the extension of the axial plateau of the Eastern Cordillera. The erosional contrast between the two morphologic domains of the Eastern Cordillera was primarily driven by the increase in the orogen regional slope by progressive accumulation of crustal shortening and thickening. Local climate, tectonics and rock type play a secondary role in controlling the erosion rates and the basin dynamics at a local scale.

Comparison of the TCN-derived erosion rates with the geomorphic digital parameters show positive correlations with SSP and/or Mx. Using our derived Equation (4) the Mx-erosion rate plot for the Eastern Cordillera can be applied to help acquire first-order estimates of erosion rates in areas where there are similar lithologic (layered sedimentary rocks in alternating competent and incompetent formations) and pluviometric characteristics (but where no TCN data are available

Acknowledgments—This work was financed by Spanish MINECO projects CGL2010-15416 and CGL2014-54180-P. L. Struth was supported by a FPI PhD grant (BES-2011-050262) from MECD (Spain). The stay at the University of Cincinnati for TCN analysis was supported by MECD grant EEBB-I-14-08485. We thank Sarah Hammer for laboratory assistance in the University of Cincinnati, and Andrés Mora, Andrés Valencia, Eliseo Tesón and Maria Luisa Arboleya for assistance and discussion during fieldwork. We thank the two anonymous reviewers of the manuscript for very constructive comments that significantly improved the original text.

References

Akaike H. 1974. A new look at the statistical model identification. *IEEE Transactions on Automatic Control* **19**: 716–723. DOI:10.1109/TAC.1974.1100705.

Andriessen PAM, Helmens KF, Hooghiemstra H, Riezebos PA, Van der Hammen T. 1993. Absolute chronology of the Pliocene-Quaternary sediment sequence of the Bogota area, Colombia. *Quaternary Science Reviews* **12**: 483–501. DOI:10.1016/0277-3791(93)90066-U.

Babault J, Van Den Driessche J, Teixell A. 2012. Longitudinal to transverse drainage network evolution in the High Atlas (Morocco): the role of tectonics. *Tectonics* **31**. DOI:10.1029/2011TC003015.

Babault J, Teixell A, Struth L, Driessche J Van Den, Arboleya M, Tesón E. 2013. Shortening, structural relief and drainage evolution in inverted rifts: insights from the Atlas Mountains, the Eastern Cordillera of Colombia and the Pyrenees. *Geological Society of London, Special Publication* **377**: 141–158. DOI: 10.1144/SP377.14

Bagnold RA. 1966. An approach to the sediment transport problem from general physics. *US Geological Survey Geological Survey Professional Paper* **422**(1): 37.

Balco G, Stone JO, Lifton N, Dunai TJ. 2008. A complete and easily accessible means of calculating surface exposure ages or erosion rates from 10Be and 26Al measurements. *Quaternary Geochronology* **3**: 174–195. DOI:10.1016/j.quageo.2007.12.001.

Bayona G, Cortes M, Jaramillo C, Ojeda G, Aristizabal JJ, Reyes-Harker a. 2008. An integrated analysis of an orogen-sedimentary basin pair: latest cretaceous-cenozoic evolution of the linked Eastern Cordillera orogen and the Llanos foreland basin of Colombia. *Geological Society of America Bulletin* **120**: 1171–1197. DOI: 10.1130/B26187.1

Bierman PR, Coppersmith R, Hanson K, Neveling J, Portenga EW, Rood DH. 2014. A cosmogenic view of erosion, relief generation, and the age of faulting in southern Africa. *GSA Today* **24**: 4–11. DOI:10.1130/GSATG206A.1.

Bonnet S. 2009. Shrinking and splitting of drainage basins in orogenic landscapes from the migration of the main drainage divide. *Nature Geoscience* **2**: 766–771. DOI:10.1038/ngeo666.

Bookhagen B, Strecker MR. 2008. Orographic barriers, high-resolution TRMM rainfall, and relief variations along the eastern Andes. *Geophysical Research Letters* **35**: 1–6. DOI:10.1029/2007GL032011.

Bookhagen B, Strecker MR. 2012. Spatiotemporal trends in erosion rates across a pronounced rainfall gradient: examples from the southern Central Andes. *Earth and Planetary Science Letters* **327–328**: 97–110. DOI:10.1016/j.epsl.2012.02.005.

Borchers B, Marrero S, Blaco G, Caffee M, Goehring B, Lifton N, Nishiizumi K, Philips F, Schaefer J, Stone J. 2016. Geological calibration of spallation production rates in the CRONUS earth project. *Quaternary Geochronology* **31**: 188–198. DOI:10.1016/j.quageo.2015.01.009.

Bourlès DL. 1988. *Etude de la géochimie de l'isotope cosmogénique 10Be et de son isotope stable 9Be en milieu océanique*. Application à la datation des sediments marins.

Brown ET, Brook EJ, Raisbeck GM, Yiou F, Kurz MD. 1992. Al in quartz: implications for exposure age dating. *Geophysical Research Letters* **19**: 369. DOI:10.1029/92GL00266.

Brown ET, Edmond JM, Raisbeck GM, Yiou F, Kurz MD, Brook EJ. 1991. Examination of surface exposure ages of Antarctic moraines using in situ produced 10Be and 26Al. *Geochimica et Cosmochimica Acta* **55**: 2269–2283. DOI:10.1016/0016-7037(91)90103-C.

Burnham KP, Anderson DR. 2002. *Model Selection and Multimodel Inference: A Practical Information – Theoretic Approach*, 2nd edn. Springer-Verlag: New York; 488. ISBN:0–387–95364-7.

Caballero V, Mora A, Quintero I, Blanco V, Parra M, Rojas LE, Lopez C, Sánchez N, Horton BK, Stockli D, Duddy I. 2013a. Tectonic controls on sedimentation in an intermontane hinterland basin adjacent to inversion structures: the Nuevo Mundo syncline, Middle Magdalena Valley, Colombia. *Geological Society, London, Special Publications* **377**: 315–342. DOI:10.1144/SP377.12.

Caballero V, Parra M, Mora A, Lopez C, Rojas LE, Quintero I. 2013b. Factors controlling selective abandonment and reactivation in thick-skin orogens: a case study in the Magdalena Valley, Colombia. *Geological Society, London, Special Publications* **377**: 343–367. DOI:10.1144/SP377.4.

Carretier S, Regard V, Vassallo R, Martinod J, Christophoul F, Gayer E, Audin L, Lagene C. 2015. A note on 10Be-derived mean erosion rates in catchments with heterogeneous lithology: examples from the western Central Andes. *Earth Surface Processes and Landforms* **40**: 1719–1729. DOI:10.1002/esp.3748.

Castelltort S, Goren L, Willett SD, Champagnac J-D, Herman F, Braun J. 2012. River drainage patterns in the New Zealand Alps primarily controlled by plate tectonic strain. *Nature Geoscience* **5**: 744–748. DOI:10.1038/ngeo1582.

Castro E. 1992. Estado actual de investigación en la cuenca del río Chicamocha, Departamentos de Santander y Boyaca. Ministerio de Minas y Energía. Instituto de investigaciones en geociencias, minería y química. Oficina regional nororiente.

Cerling TE, Craig H. 1994. Geomorphology and *in situ* cosmogenic isotopes. *Annual Review of Earth and Planetary Sciences* **22**: 273–317. DOI:10.1146/annurev.earth.22.1.273.

Chadwick OA, Roering JJ, Heimsath AM, Levick SR, Asner GP, Khomo L. 2013. Shaping post-orogenic landscapes by climate and chemical weathering. *Geology* **41**: 1171–1174. DOI:10.1130/G34721.1.

Colletta B, Hebrard F, Letouzey J, Werner P, Rudkiewicz J-R. 1990. Tectonic style and crustal structure of the Eastern Cordillera (Colombia) from a balanced cross-section. In *Petroleum and Tectonics in Mobile Belts: 4th IFP Exploration and Production Research Conference*, Bordeaux, 1988 (Design Guides for Offshore Structures), 81–100.

Cooper M, Addison FT, Alvares R, Hayward B, Howe S, Pulham J, Taborda A. 1995. Basin development and tectonic history of the Llanos basin. *Colombia. Petroleum basins of South America. AAPG. Memoir no.* **62**(10): 659–666.

Corbett LB, Bierman PR, Rood DH. 2013. Optimizing sample preparation for high precision, low-detection limit analysis of in situ 10Be: Strategies and new data. *Geological Society of America Abstracts with Programs* **45**.

Dibiase RA, Whipple KX, Heimsath AM, Ouimet WB. 2010. Landscape form and millennial erosion rates in the San Gabriel Mountains, CA. *Earth and Planetary Science Letters* **289**: 134–144. DOI:10.1016/j.epsl.2009.10.036.

Dortch JM, Owen LA, Haneberg WC, Caffee MW, Dietsch C, Kamp U. 2009. Nature and timing of large landslides in the Himalaya and Transhimalaya of northern India. *Quaternary Science Reviews* **28**: 1037–1054. DOI:10.1016/j.quascirev.2008.05.002.

Dortch JM, Owen LA, Schoenbohm LM, Caffee MW. 2011. Asymmetrical erosion and morphological development of the central Ladakh Range, northern India. *Geomorphology* **135**: 167–180. DOI:10.1016/j.geomorph.2011.08.014.

Godard V, Burbank DW, Bourls DL, Bookhagen B, Braucher R, Fisher GB. 2012. Impact of glacial erosion on 10Be concentrations in fluvial sediments of the Marsyandi catchment, central Nepal. *Journal of Geophysical Research - Earth Surface* **117**. DOI:10.1029/2011JF002230.

Gómez E, Jordan TE, Allmendinger RW, Hegarty K, Kelley S. 2005. Syntectonic Cenozoic sedimentation in the northern middle Magdalena Valley Basin of Colombia and implications for exhumation of the Northern Andes. *Bulletin of the Geological Society of America* **117**: 547–569. DOI:10.1130/B25454.1.

González JV, Jiménez G. 2015. *Análisis estructural y características microtectónicas de un segmento de la falla Bucaramanga en los alrededores del corregimiento Umpalá, Santander.* Universidad Industrial de Santander, Bucaramanga.

Goren L, Willett SD, Herman F, Braun J. 2014. Coupled numerical-analytical approach to landscape evolution modeling. *Earth Surface Processes and Landforms* **39**: 522–545. DOI:10.1002/esp.3514.

Granger DE, Kirchner JW, Finkel R. 1996. Spatially averaged long-term erosion rates measured from *in situ*-produced cosmogenic nuclides in alluvial sediment. *The Journal of Geology* **104**: 249–257. DOI:10.1086/629823.

Horton BK, Saylor JE, Nie J, Mora A, Parra M, Reyes-Harker A, Stockli DF. 2010. Linking sedimentation in the northern Andes to basement configuration, Mesozoic extension, and Cenozoic shortening: evidence from detrital zircon U–Pb ages, Eastern Cordillera, Colombia. *Bulletin of the Geological Society of America* **122**: 1423–1442. DOI:10.1130/B30118.1.

Howard AD. 1965. Geomorphological systems – equilibrium and dynamics No Title. *American Journal of Science* **263**: 302–312.

Howard AD, Dietrich WE, Seidl MA. 1994. Modeling fluvial erosion on regional to continental scales. *Journal of Geophysical Research* **99**: 13971–13986. DOI:10.1029/94JB00744.

Howard AD, Kerby G. 1983. Channel changes in badlands. *Geological Society of America Bulletin* **94**: 739–752.

Hurvich C, Tsai C. 1989. Regression and time series model selection in small samples. *Biometrika* **76**: 297–307. DOI:10.1093/biomet/76.2.297.

Jarvis A, Reuter HI, Nelson A, Guevara E. 2008. Hole-filled SRTM for the globe. Version 4. http://srtm.csi.cgiar.org

Julivert M. 1963. Los rasgos tectónicos de la región de la Sabana de Bogotá y los mecanismos de la formación de las estructuras. *Boletín de Geología Universidad Industrial Santander* **13–14**: 5–102.

Julivert M. 1970. Cover and basement tectonics in the cordillera oriental of Colombia, South America, and a comparison with some other folded chains. *Geological Society of America Bulletin* **81**: 3623–3646.

Kirby E, Whipple K. 2001. Quantifying differential rock-uplift rates via stream profile analysis. *Geology* **6**: 415–418.

Kirby E. 2003. Distribution of active rock uplift along the eastern margin of the Tibetan Plateau: Inferences from bedrock channel longitudinal profiles. *Journal of Geophysical Research* **108**: 2217. DOI:10.1029/2001JB000861.

Kirby E, Whipple KX. 2012. Expression of active tectonics in erosional landscapes. *Journal of Structural Geology* **44**: 54–75. DOI:10.1016/j.jsg.2012.07.009.

Knighton AD. 1999. Downstream variation in stream power. *Geomorphology* **29**: 293–306.

Kohl CP, Nishiizumi K. 1992. Chemical isolation of quartz for measurement of *in situ*-produced cosmogenic nuclides. *Geochimica et Cosmochimica Acta* **56**: 3583–3587. DOI: 10.1016/0016-7037(92)90401-4

Lal D. 1991. Cosmic ray labeling of erosion surfaces: *in situ* nuclide production rates and erosion models. *Earth and Planetary Science Letters* **104**: 424–439. DOI:10.1016/0012-821X(91)90220-C.

Lal D, Arnold JR. 1985. Tracing quartz through the environment. *Proceedings of the Indian Academy of Sciences - Earth and Planetary Sciences* **94**: 1–5. DOI:10.1007/BF02863403.

Marrero SM, Phillips FM, Borchers B, Lifton N, Aumer R, Balco G. 2016. Cosmogenic nuclide systematic and the CRONUScalc program. *Quaternary Geochronology* **31**: 160–187. DOI:10.1016/j.quageo.2015.09.005.

Mora A, Horton BK, Mesa A, Rubiano J, Ketcham RA, Parra M, Blanco V, Garcia D, Stockli DF. 2010. Migration of Cenozoic deformation in the Eastern Cordillera of Colombia interpreted from fission track results and structural relationships: implications for petroleum systems. *AAPG Bulletin* **94**: 1543–1580. DOI:10.1306/01051009111.

Mora A, Parra M, Strecker MR, Sobel ER, Hooghiemstra H, Torres V, Jaramillo JV. 2008. Climatic forcing of asymmetric orogenic evolution in the Eastern Cordillera of Colombia. *Bulletin of the Geological Society of America* **120**: 930–949. DOI:10.1130/B26186.1.

Moreno CJ, Horton BK, Caballero V, Mora A, Parra M, Sierra J. 2011. Depositional and provenance record of the Paleogene transition from foreland to hinterland basin evolution during Andean orogenesis, northern Middle Magdalena Valley Basin, Colombia. *Journal of South American Earth Sciences* **32**: 246–263. DOI:10.1016/j.jsames.2011.03.018.

Mudd SM, Attal M, Milodowski DT, Grieve SWD, Valters DA. 2014. A statistical framework to quantify spatial variation in channel gradients using the integral method of channel profile analysis. *Journal of Geophysical Research - Earth Surface* **119**: 138–152. DOI:10.1002/2013JF002981.

Niemi NA, Oskin M, Burbank DW, Heimsath AM, Gabet EJ. 2005. Effects of bedrock landslides on cosmogenically determined

erosion rates. *Earth and Planetary Science Letters* **237**: 480–498. DOI:10.1016/j.epsl.2005.07.009.

Nishiizumi K, Imamura M, Caffee MW, Southon JR, Finkel RC, McAninch J. 2007. Absolute calibration of 10Be AMS standards. *Nuclear Instruments and Methods in Physics Research, Section B: Beam Interactions with Materials and Atoms* **258**: 403–413. DOI:10.1016/j.nimb.2007.01.297.

Parra M, Mora A, Jaramillo C, Strecker MR, Sobel ER, Quiroz L, Rueda M, Torres V. 2009a. Orogenic wedge advance in the northern Andes: evidence from the Oligocene-Miocene sedimentary record of the Medina Basin, Eastern Cordillera, Colombia. *Bulletin of the Geological Society of America* **121**: 780–800. DOI:10.1130/B26257.1.

Parra M, Mora A, Jaramillo C, Torres V, Zeilinger G, Strecker MR. 2010. Tectonic controls on Cenozoic foreland basin development in the north-eastern Andes, Colombia. *Basin Research* **22**: 874–903. DOI:10.1111/j.1365-2117.2009.00459.x.

Parra M, Mora A, Sobel ER, Strecker MR, González R. 2009b. Episodic orogenic front migration in the northern Andes: constraints from low-temperature thermochronology in the Eastern Cordillera, Colombia. *Tectonics* **28**. DOI:10.1029/2008TC002423.

Pelletier JD. 2004. Persistent drainage migration in a numerical landscape evolution model. *Geophysical Research Letters* **31** : L20501. DOI:10.1029/2004GL020802.

Perron JT, Richardson PW, Ferrier KL, Lapôtre M. 2012. The root of branching river networks. *Nature* **492**: 100–103. DOI:10.1038/nature11672.

Perron JT, Royden L. 2013. An integral approach to bedrock river profile analysis. *Earth Surface Processes and Landforms* **38**: 570–576. DOI:10.1002/esp.3302.

Portenga EW, Bierman PR, Duncan C, Corbett LB, Kehrwald NM, Rood DH. 2015. Erosion rates of the Bhutanese Himalaya determined using in situ-produced 10Be. *Geomorphology* **233**: 112–126. DOI:10.1016/j.geomorph.2014.09.027.

Pupim N, Bierman PR, Luis M, Rood DH, Silva A, Renato E. 2015. Geomorphology erosion rates and landscape evolution of the lowlands of the Upper Paraguay river basin (Brazil) from cosmogenic 10 Be. *Geomorphology* **234**: 151–160. DOI:10.1016/j.geomorph.2015.01.016.

Royden L, Taylor Perron J. 2013. Solutions of the stream power equation and application to the evolution of river longitudinal profiles. *Journal of Geophysical Research Earth Surface* **118**: 497–518. DOI:10.1002/jgrf.20031.

Safran EB, Bierman PR, Aalto R, Dunne T, Whipple KX, Caffee M. 2005. Erosion rates driven by channel network incision in the Bolivian Andes. *Earth Surface Processes and Landforms* **30**: 1007–1024. DOI:10.1002/esp.1259.

Salgado AAR, Braucher RV, Colin F, Varajão AFDC, Nalini HA, Jr. 2008. Relief evolution of the Quadrilátero Ferrífero (Minas Gerais, Brazil) by means of (10Be) cosmogenic nuclei. *Zeitschrift für Geomorphologie* **52**: 317–323. DOI:10.1127/0372-8854/2008/0052-0317.

Saylor JE, Horton BK, Nie J, Corredor J, Mora A. 2011. Evaluating foreland basin partitioning in the northern Andes using Cenozoic fill of the Floresta basin, Eastern Cordillera, Colombia. *Basin Research* **23**: 377–402. DOI:10.1111/j.1365-2117.2010.00493.x.

Segovia A. 1965. *Mapa Geológico de la plancha L-12 (Medina)*, de la República de Colombia, Bogotá.

Silva A, Mora A, Caballero V, Rodriguez G, Ruiz C, Moreno N, Parra M, Ramirez-Arias JC, Ibanez M, Quintero I. 2013. Basin compartmentalization and drainage evolution during rift inversion: evidence from the Eastern Cordillera of Colombia. *Geological Society, London, Special Publications* **377**: 369–409. DOI:10.1144/SP377.15.

Snyder NP, Whipple KX, Tucker GE, Merritts DJ. 2003. Channel response to tectonic forcing: field analysis of stream morphology and hydrology in the Mendocino triple junction region, northern California. *Geomorphology* **53**: 97–127. DOI:10.1016/S0169-555X(02)00349-5.

Stone JO. 2000. Air pressure and cosmogenic isotope production. *Journal of Geophysical Research* **105**: 23753. DOI:10.1029/2000JB900181.

Struth L, Babault J, Teixell A. 2015. Drainage reorganization during mountain building in the river system of the Eastern Cordillera of the Colombian Andes. *Geomorphology* **250**: 370–383. DOI:10.1016/j.geomorph.2015.09.012.

Teixell A, Tesón E, Ruiz JC, Mora A. 2015. The structure of an inverted back-arc rift: insights from a transect across the Eastern Cordillera of Colombia near Bogotá. In *Petroleum Geology and Hydrocarbon Potential of Colombia Caribbean Margin: AAPG Memoir 108*, Bartolini C, Mann P (eds), 499–516.

Tesón E, Mora A, Silva A, Namson J, Teixell A, Castellanos J, Casallas W, Julivert M, Taylor M, Ibáñez-Mejía M, Valencia VA. 2013. Relationship of Mesozoic graben development, stress, shortening magnitude, and structural style in the Eastern Cordillera of the Colombian Andes. *Geological Society, London, Special Publications* **377**: 257–283. DOI:10.1144/SP377.10.

Torres V, Vandenberghe J, Hooghiemstra H. 2005. An environmental reconstruction of the sediment infill of the Bogotá basin (Colombia) during the last 3 million years from abiotic and biotic proxies. *Palaeogeography, Palaeoclimatology, Palaeoecology* **226**: 127–148. DOI:10.1016/j.palaeo.2005.05.005.

Ulloa C, Rodríguez E. 1979. Geología del Cuadrángulo K12, Ingeominas-Boletín Geológico **22**(1): 1–55.

Ulloa C, Rodriguez GI. 1982. *Intrusiones ácidas ordovícicas y post-devónicas en Floresta (Boyacá)*. Resum IV Congr. Colombiano Geol. Cali

Van der Beek P, Champel B, Mugnier JL. 2002. Control of detachment dip on drainage development in regions of active fault-propagation folding. *Geology* **30**: 471–474. DOI:10.1130/0091-7613(2002)030<0471:CODDOD>2.0.CO;2.

Viaplana M, Babault J, Dominguez S, Van Den Driessche J, Legrand X. 2015. Drainage network evolution and patterns of sedimentation in an experimental wedge. *Tectonophysics* **664**: 109–124. DOI:10.1016/j.tecto.2015.09.007.

Von Blanckenburg F. 2005. The control mechanisms of erosion and weathering at basin scale from cosmogenic nuclides in river sediment. *Earth and Planetary Science Letters* **237**: 462–479. DOI:10.1016/j.epsl.2005.06.030.

Whipple KX, Tucker GE. 1999. Dynamics of the stream-power river incision model: implications for height limits of mountain ranges, landscape response timescales, and research needs. *Journal of Geophysical Research* **104**: 17661–17674. DOI:10.1029/1999JB900120.

Willett SD, McCoy SW, Perron JT, Goren L, Chen C-Y. 2014. Dynamic reorganization of river basins. *Science* (New York, NY) 343: DOI: 10.1126/science.1248765

Willett SD, Slingerland R, Hovius N. 2001. Uplift, shortening, and steady-state topography in active mountain belts. *American Journal of Science* **301**: 455–485. DOI:10.2475/ajs.301.45.455.

Wobus C, Whipple KX, Snyder N, Johnson J, Sheehan D. 2006. Tectonics from topography: Procedures, promise, and pitfalls. *GSA Special Papers* **398**: 55–74. https://doi.org/10.1130/2006.2398(04).

Yang R, Willett SD, Goren L. 2015. *In situ* low-relief landscape formation as a result of river network disruption. *Nature* **520**: 526–529. DOI:10.1038/nature14354.

Yanites BJ, Tucker GE, Anderson RS. 2009. Numerical and analytical models of cosmogenic radionuclide dynamics in landslide-dominated drainage basins. *J. Geophysical Research* **114**: F01007. DOI:10.1029/2008JF001088.

Supporting Information

Additional supporting information may be found in the online version of this article at the publisher's web site.

Figure S1. Supporting info item